

# An Organometallic Sandwich Lanthanide Single-Ion Magnet with an Unusual Multiple Relaxation Mechanism

Matthew Jeletic, Po-Heng Lin, Jennifer J. Le Roy, Ilia Korobkov, Serge I. Gorelsky, and Muralee Murugesu\*

Chemistry Department and the Centre for Catalysis Research and Innovation, University of Ottawa, 10 Marie Curie, Ottawa, ON, Canada K1N 6N5

**S** Supporting Information

**ABSTRACT:** A dysprosium(III) sandwich complex,  $[\text{Dy}^{\text{III}}(\text{COT}'')_2\text{Li}(\text{THF})(\text{DME})]$ , was synthesized using 1,4-bis(trimethylsilyl)cyclooctatetraenyl dianion ( $\text{COT}''$ ). The complex behaves as a single-ion magnet and demonstrates unusual multiple relaxation modes. The observed relaxation pathways strongly depend on the applied static dc fields.

Since discovering that  $\text{Mn}_{12}\text{OAc}^1$  exhibits slow magnetic relaxation intrinsic to magnetlike behavior, hundreds of new coordination complexes have been reported as single-molecule magnets (SMMs).<sup>2</sup> Such unique magnetic behavior originates from a combination of a large spin ground state ( $S$ ) and uniaxial magnetic anisotropy ( $D$ ). Single-ion magnets (SIMs)<sup>3</sup> represent a special class of magnetic molecules in which slow relaxation of the magnetization arises from a single metal center. Among the numerous reported mononuclear lanthanide complexes, only a select few behave as SIMs.<sup>3a–n</sup> In such molecules, although the total number of unpaired electrons is limited, the intrinsic magnetic anisotropy can be significant and has led to mononuclear complexes with remarkably high energy barriers.<sup>3b,i</sup> In theory, isolating complexes with large  $D$  and reduced rhombic anisotropy ( $E$ ) leads to large energy barriers to magnetization reversal.<sup>3k–m</sup> In SMMs and SIMs, reversal of the spin occurs via a thermal pathway and/or a quantum tunneling of the magnetization (QTM) pathway. Both the thermally activated and quantum regimes are often clearly observed in lanthanide SIMs, but multiple relaxation regimes are rare and not well understood. This is mainly due to multiple energy levels close in energy providing closely located spin-reversal pathways, leading to overlapping relaxation mechanisms. Therefore, isolating complexes with well-defined multiple relaxation modes is challenging. Moreover, controlling the multiple relaxation pathways via an external stimulus (e.g., fields, light) would undoubtedly not only enhance our knowledge of such unusual relaxation mechanisms but also provide new ways to improve the properties of SMMs. Relaxation mechanism in SIMs are often induced by the ligand field, as the coordinating ligands directly influence the axial or rhombic terms.<sup>3k–m</sup> Therefore, choosing an appropriate ligand system is key. Most reported SIMs are coordination complexes, with only two examples of purely organometallic structures.<sup>3i,p</sup> The magnetism of lanthanide metal-locenes is virtually unknown but provides a great platform for studying ligand-field effects on magnetic properties.<sup>2a,3i,4</sup>

With this in mind, we focused our attention toward the synthesis and study of dysprosium sandwich complexes containing 1,4-bis(trimethylsilyl)cyclooctatetraenyl dianion ( $\text{COT}''$ ) as the ligands. Evans, Edelmann, and others have elegantly demonstrated that COT ligands are ideal for isolating sandwich-type complexes with 4f elements.<sup>5</sup> We believe the interaction between the 4f orbitals of the metal and the  $\pi$  orbitals of the  $\text{COT}''$  ligands may play a key role in the ligand field, thereby enhancing the magnetic properties. Herein we report a new organodysprosium(III) complex that acts as a SIM and displays unusual relaxation processes where multiple relaxation pathways result from a single metal.

The reaction of 2 equiv of  $\text{DyCl}_3$  with 3 equiv of  $\text{COT}''$ - $(\text{LiTHF}_2)_2$ <sup>6</sup> in tetrahydrofuran (THF) for 48 h at room temperature provided fine needles of **1** that crystallizes in the monoclinic space group  $P2_1/c$ . The molecular structure consists of two  $\text{COT}''$  ligands  $\eta^8$ -bound to the central  $\text{Dy}^{\text{III}}$  ion with a Dy–C bond distance range of 2.6–2.7 Å (Figure 1). To accommodate the sterically bulky trimethylsilyl groups, the sandwiching  $\text{COT}''$  rings are arranged in a staggered conformation (Figure S1 in the Supporting Information). A Li ion interacts with one  $\text{COT}''$  ring (Li– $\text{C}_{\text{COT}''}$  distances between 2.33 and 2.51 Å). Such a structure is consistent with weak Li– $\text{COT}''$  interactions through the  $\pi$  cloud of the  $\text{COT}''$  ring.<sup>7</sup> The distance between the  $\text{COT}''$  centroids and the  $\text{Dy}^{\text{III}}$  center are 1.93 Å (lithiated  $\text{COT}''$ ) and 1.87 Å. The small difference in these distances arises from withdrawal of electron density out of the lithiated  $\text{COT}''$  ring by the Li, resulting in a longer Dy–centroid bond. The two  $\text{COT}''$  rings are in a nearly parallel arrangement with a slight tilt angle of 3.59° (Figure S1). One THF and one DME molecule also coordinate around the Li ion. The Li–C bond is considerably longer than the Li–O bonds (THF, 1.86 Å; DME, 1.99 and 2.01 Å), also supporting the Li–C binding mode. Structure **1** also contains three disorders: one in the THF molecule attached to the Li center, another in the silyl groups attached to the nonlithiated  $\text{COT}''$  ring, and the third in the toluene molecule of crystallization. Lastly, the  $\text{C}_{\text{COT}''}$ –Si bond lengths are 1.87, 1.87, 1.88, and 1.87 Å. Detailed inspection of the packing arrangement reveals that the closest intermolecular  $\text{Dy} \cdots \text{Dy}$  distance is 10.1 Å (Figure S2).

Several reports have suggested that the f  $\delta$  orbital and  $\pi$  orbitals are likely to have an impact on the  $\text{M}(\text{COT})_2$  electronic interactions.<sup>8</sup> Therefore, to probe the electronic structure of complex **1**, density functional theory calculations at the spin-unrestricted B3LYP<sup>9</sup>/TZVP<sup>10</sup> level (using the SDD basis set<sup>11</sup>

**Received:** August 19, 2011

**Published:** October 27, 2011

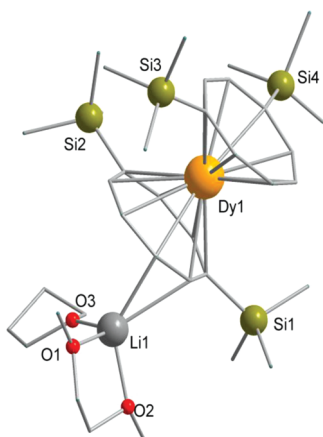


**Figure 1.** X-ray structure of  $[\text{Dy}^{\text{III}}(\text{COT}'')_2\text{Li}(\text{THF})(\text{DME})]$  (**1**). Selected bond distances (Å) and angles (deg): Dy–C<sub>COT''</sub>, 2.6–2.7; Li–C<sub>COT''</sub>, 2.33–2.51; C–C, 1.40–1.42; X<sub>COT''</sub>–X<sub>COT''</sub>, 3.79; COT''–COT'' tilt angle, 3.59; X<sub>COT''</sub>–Dy–X<sub>COT''</sub>, 168.16. X<sub>COT''</sub> = ring center. Color code: Dy<sup>III</sup>, orange; Li, gray; O, red; Si, green. H atoms have been omitted for clarity.

and effective core potential for Dy) were conducted using the crystal-structure geometry. The silyl groups were replaced by protons, and all C–H bond distances were adjusted from the X-ray structure values to 1.07 Å. The optimized wave function for the ground state ( $S = 5/2$ ) was used to evaluate the bonding contributions. Figure 2 displays the spin density of the ground state. The Dy atom carries a spin density of 5.51 au due to five singly occupied 4f orbitals of Dy<sup>III</sup>, while the COT ligands demonstrate significant spin polarization (a spin density of 0.26 au with the opposite sign to the neighboring Dy atom). This is due to a difference in charge donation from the dianionic COT ligands to Dy<sup>III</sup> through  $\alpha$  and  $\beta$  spin orbitals. Overall, each dianionic COT ligand donates  $\sim 1.2 e^-$  to Dy<sup>III</sup>, resulting in the +0.58 au charge for the Dy atom.

The Mayer bond order<sup>12</sup> between Dy and each COT ligand is 1.67, with  $\alpha$ - and  $\beta$ -spin occupied orbitals contributing 0.90 and 0.77, respectively, to the total metal–ligand bond order. The analysis of the wave function in terms of contributions from fragment orbitals indicated that only charge donation from the COT ligands to Dy<sup>III</sup> contributes to the covalent bonding in the complex. Five occupied  $\pi$  orbitals of the dianionic COT ligands (HOMO, HOMO–1, HOMO–2, HOMO–3, and HOMO–5) participate significantly (change in orbital population > 3%) in covalent bonding with the Dy<sup>III</sup> ion.

To investigate the magnetic properties of **1**, direct current (dc) susceptibility measurements were carried out on a freshly prepared sample (under nitrogen) under an applied field of 0.1 T over the 2.5–300 K temperature range (Figure S3). The room-temperature  $\chi T$  value of  $14.7 \text{ cm}^3 \text{ K mol}^{-1}$  for **1** is in good agreement with the expected theoretical value of  $14.17 \text{ cm}^3 \text{ K mol}^{-1}$  for a Dy<sup>III</sup> ( $^6\text{H}_{15/2}$ ,  $S = 5/2$ ,  $L = 5$ ,  $g = 4/3$ ) ion. The  $\chi T$  product remains constant with decreasing temperature until  $\sim 20$  K, where it decreases sharply and reaches a minimum value of  $10.6 \text{ cm}^3 \text{ K mol}^{-1}$  at 2.5 K. Such behavior is consistent with that of previously reported mononuclear Ln<sup>III</sup> complexes.<sup>3</sup> The low-temperature decrease is most likely due to the large inherent magnetic anisotropy of the Dy<sup>III</sup> ion, but depopulation of the excited states in conjunction with weak intermolecular interactions cannot be ruled out. The  $M$ -versus- $H/T$  plot below 10 K

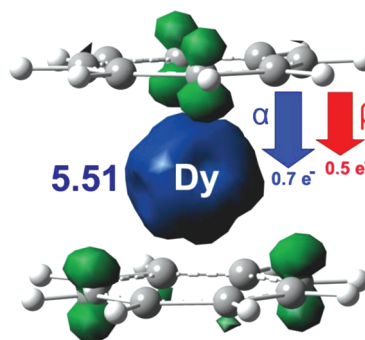


**Figure 2.** Spin density distribution of the ground state ( $S = 5/2$ ) of  $[\text{Dy}(\text{COT})_2]^-$  **1**. Blue and green regions indicate positive and negative spin density, respectively. Blue and red arrows indicate charge donation from one dianionic COT ligand to Dy<sup>III</sup> through  $\alpha$  and  $\beta$  spin orbitals, respectively.

(Figure S4) displays a rapid increase in the magnetization at low fields. At higher fields,  $M$  increases linearly without saturation even at 7 T. The latter variation at high fields and the non-superposition of the isofield lines on a single master curve indicates the presence of significant magnetic anisotropy and/or low-lying excited states in **1**. In addition, the  $M$ -versus- $H$  data do not reveal a hysteresis loop with the sweep rates and temperature range attainable with our traditional SQUID magnetometer.

The magnetization relaxation dynamics was studied using alternating current (ac) magnetic susceptibility measurements (temperature range 2.5–15 K with a zero dc field and a 3.5 Oe ac field oscillating at frequencies of 1–1500 Hz) to probe the SIM behavior of **1**. The data reveal strong frequency-dependent out-of-phase ( $\chi''$ ) and in-phase ( $\chi'$ ) signals below 14 K (Figure 3 and Figure S5). The intensities of the signals increase with decreasing temperature and frequency. Such behavior clearly indicates slow relaxation of the magnetization associated with SIM behavior. Figure S5 illustrates a relaxation peak for temperatures between 2.5 and 8 K with a peak maximum at 5.8 K for 1500 Hz. A peak tail at low temperatures indicates the presence of QTM at zero field. Additionally, the ac susceptibility as a function of frequency over the same temperature range (Figure 3 top) confirms the classic SIM traits of **1**, signaled by the shape of the frequency-dependent signal. In fact, as  $T$  decreases to 3.75 K, a gradual shift of the peak maximum toward lower frequency occurs (pathway A). Below 3.75 K, relaxation starts to become temperature-independent, indicative of a quantum regime (pathway B). Analysis of the frequency-dependent data using the Arrhenius law [ $\tau = \tau_0 \exp(U_{\text{eff}}/k_{\text{B}}T)$ ] gave a calculated relaxation barrier of  $U_{\text{eff}} = 18$  K and a  $\tau_0$  value of  $6 \times 10^{-6}$  s for the high-temperature thermally activated region (A<sub>0</sub>) (Figure 4). The barrier is relatively small as a result of the QTM.

Since applying a static dc field reduces the QTM through the spin-reversal barrier via degenerate  $\pm M_s$  energy levels, measurements at various applied dc fields should lift the degeneracy (Figure S6).<sup>21</sup> In the plot of  $\chi''$  versus  $\nu$  at 3 K, the peak with a maximum at 345 Hz at 0 Oe slightly decreases and shifts to 277 Hz at 200 Oe and disappears at dc fields above 300 Oe. Therefore, optimizing the field minimizes the QTM at 3 K (in this case at 600 Oe). It is noteworthy that while the peak is decreasing, the appearance of a secondary peak at 100 Oe becomes evident, indicating a possible thermally activated secondary relaxation

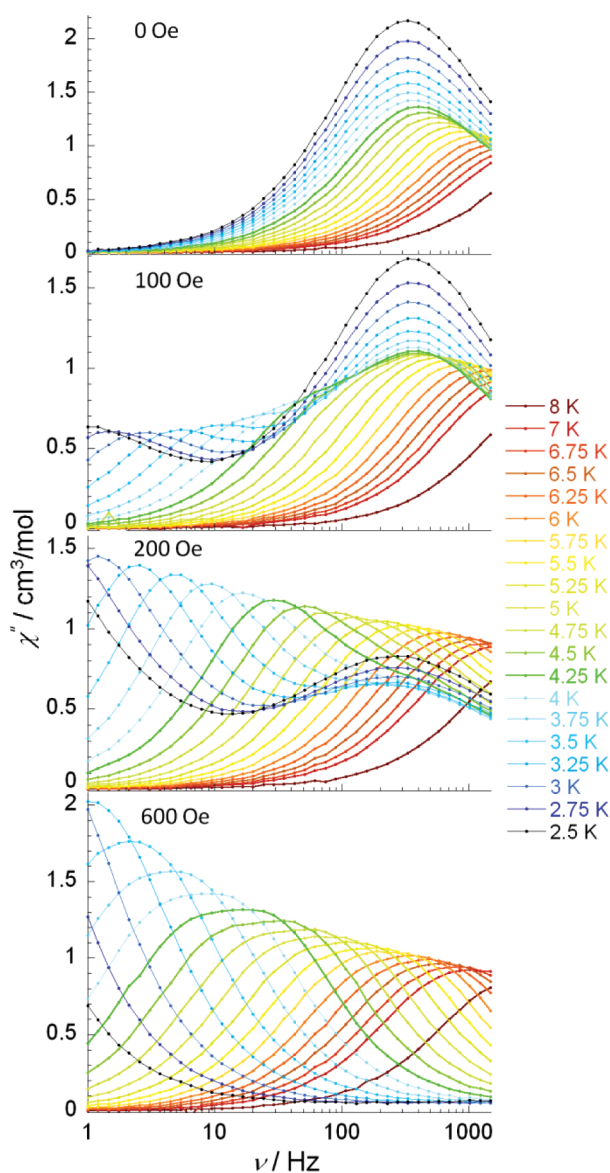


**Figure 3.** Frequency dependence of the out-of-phase ac susceptibility ( $\chi''$ ) of **1** from 2.5 to 8 K at the indicated applied dc fields.

pathway (pathway C). The unusual multiple relaxation mechanisms become evident in a comparison of the ac susceptibility data at dc fields of 0, 100, 200, and 600 Oe (optimum) (Figure 3 and Figures S7–S10). Applying a 100 Oe field results in a reduction in the quantum tunneling (i.e., a decrease in the frequency-dependent tail; Figures S7–S9) along with the appearance of the aforementioned secondary peak, indicating the coexistence of the new relaxation pathway C below 100 Hz and 4.25 K. The shoulder at  $\sim 4.25$  K suggests the coalescence of the two peaks, signaling that pathways A and C are equally prominent (Figure S11). At higher temperatures, thermally activated pathway A is dominant.

When the magnetization relaxation time ( $\tau$ ) is plotted as  $\ln(\tau)$  versus  $T^{-1}$  (Figure 4), two thermally activated regimes [ $U_{\text{eff}}(\text{A}_{100}) = 24$  K,  $\tau_0 = 3 \times 10^{-6}$  s;  $U_{\text{eff}}(\text{C}_{100}) = 23$  K,  $\tau_0 = 3 \times 10^{-5}$  s) as well as the initial quantum regime are obtained for a 100 Oe measurement. At 200 Oe, the intensity of the secondary low-frequency peak (C) increases [ $U_{\text{eff}}(\text{C}_{200}) = 43$  K,  $\tau_0 = 3 \times 10^{-7}$  s] and the intensity of the primary high-frequency peak (A)

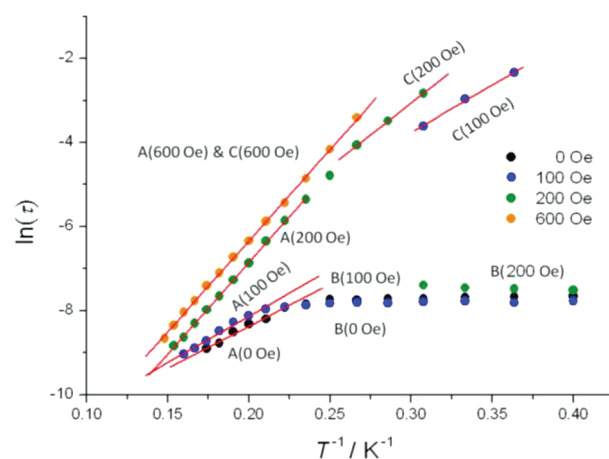


**Figure 4.** Plots of  $\ln(\tau)$  vs  $T^{-1}$  at  $H_{\text{dc}} = 0, 100, 200$ , and  $600$  Oe, representing relaxation pathways A, B, and C. The solid lines represent Arrhenius fits of the frequency-dependent data.

decreases [ $U_{\text{eff}}(\text{A}_{200}) = 30$  K,  $\tau_0 = 6 \times 10^{-6}$  s], indicating that the applied field promotes pathway C as the primary relaxation route. The data at the optimum field of 600 Oe, consistent with the other fields, continues to illustrate that the low-frequency peak C is the predominant relaxation pathway. However, close inspection of the peak shape (4.25 K data; Figure S11) reveals that the peak signals are broad, suggesting an overlapping relaxation mechanism (A and C) with very similar relaxation times. The overlapping peaks are barely apparent.

Therefore, with the assumption of a single relaxation, fitting the 600 Oe data to the Arrhenius law provides an effective energy barrier of  $U_{\text{eff}} = 43$  K with  $\tau_0 = 3 \times 10^{-7}$  s. The increase in the anisotropic barrier from 18 to 43 K simply validates that the quantum tunneling is rather significant at zero field.

A three-dimensional graphical representation of  $\chi''$  versus  $\chi'$  (a Cole–Cole plot) over the 2.5–7 K temperature range (Figure S12) further validates the existence of multiple relaxation processes. Upon application of a static dc field of 100 Oe, near semicircles become two fused semicircles below 4.25 K (Figure S12, top right). When the field is increased to 200 Oe, the switching of the intensities of the two semicircles confirms that pathway C becomes more dominant (Figure S12, bottom left). The optimum-field measurements show a broad semicircle (Figure S12, bottom right), suggesting that relaxation mechanisms A and C overlap. Fitting of the observed data to a generalized Debye model<sup>13</sup> yielded the following set of  $\alpha$  parameter ranges: 0 Oe, 0.10–0.25; 100 Oe, 0.33–0.40 and 0.002–0.37; 200 Oe, 0.65–0.87 and 0.04–0.14; 600 Oe, 0.10–0.30 Oe. These ranges indicate that the observed data reasonably fit the theoretical curves.

In conclusion, the newly discovered complex  $[\text{Dy}^{\text{III}}(\text{COT}'')_2\text{-Li}(\text{THF})(\text{DME})]$  demonstrates slow magnetic relaxation primarily caused by intrinsic single-ion anisotropy. The two COT'' ligands appear to perturb the ligand field enough to influence the anisotropy. Interestingly, multiple relaxation pathways are accessible through the application of various dc fields. Recently, Kajiwarra and co-workers proposed that a bimetallic Dy–Zn coordination complex<sup>3n</sup> has multiple relaxation pathways. However, the multiple relaxations overlapped and were unclear in the ac susceptibility data, in contrast to the results for our complex. This marks **1** as the first clear example of a system exhibiting multiple relaxation pathways arising from a single metal center in a  $\text{Ln}^{\text{III}}$  complex, let alone with an organolanthanide complex.



Evans and co-workers<sup>5a</sup> first reported the organometallic complex [(COT)Er(Cp\*)], which Gao and co-workers recently demonstrated to exhibit SIM behavior.<sup>3i</sup> The complex displays two relaxation peaks attributed to the presence of two different conformers. In contrast, our X-ray structure clearly demonstrates the presence of a single conformer yet multiple relaxation pathways. Similarly, another COT-based system exhibiting slow relaxation of the magnetization is a pure *Sf* system, [Np(COT)<sub>2</sub>], where the appearance of an ac signal occurs only under an applied dc field.<sup>3p</sup> The differences in the relaxation barriers for our systems versus [(COT)Er(Cp\*)] and [Np(COT)<sub>2</sub>] primarily arise from the intrinsic anisotropy of the metal and the ligand-field environment. To evaluate further the influence of the ligand-field effect on the complex relaxation pathways, we are currently studying analogous Dy<sup>III</sup> sandwich complexes using COT ligands with different substituents. Shortcutting and opening relaxation pathways via applied fields in a family of organolanthanide complexes is an exciting challenge that may open new avenues toward the goal of producing molecules for technologies such as quantum computation.

## ■ ASSOCIATED CONTENT

**S Supporting Information.** Complete experimental details and crystallographic data (CIF). This material is available free of charge via the Internet at <http://pubs.acs.org>.

## ■ AUTHOR INFORMATION

**Corresponding Author**  
m.murugesu@uottawa.ca

## ■ ACKNOWLEDGMENT

We thank the University of Ottawa, NSERC (Discovery and RTI Grants), CFI, and FFCR for their financial support.

## ■ REFERENCES

- (a) Sessoli, R.; Gatteschi, D.; Caneschi, A.; Novak, A. *Nature* **1993**, *45*, 141. (b) Sessoli, R.; Tsai, H.-L.; Schake, A. R.; Wang, S.; Vincent, J. B.; Folting, K.; Gatteschi, D.; Christou, G.; Hendrickson, D. N. *J. Am. Chem. Soc.* **1993**, *115*, 1804.
- (a) Layfield, R. A.; McDouall, J. J. W.; Sulway, S. A.; Tuna, F.; Collison, D.; Winpenny, R. E. P. *Chem.—Eur. J.* **2010**, *16*, 4442. (b) Lin, P.-H.; Burchell, T. J.; Clérac, R.; Murugesu, M. *Angew. Chem., Int. Ed.* **2008**, *47*, 8848. (c) Luzon, J.; Bernot, K.; Hewitt, I. J.; Anson, C. E.; Powell, A. K.; Sessoli, R. *Phys. Rev. Lett.* **2008**, *100*, No. 247205. (d) Zaleski, C. M.; Depperman, E. C.; Kampf, J. W.; Kirk, M. L.; Pecoraro, V. L. *Angew. Chem., Int. Ed.* **2004**, *43*, 3912. (e) Aronica, C.; Pilet, G.; Chastanet, G.; Wernsdorfer, W.; Jacquot, J.-F.; Luneau, D. *Angew. Chem., Int. Ed.* **2006**, *45*, 4659. (f) Costes, J.-P.; Shova, S.; Wernsdorfer, W. *Dalton Trans.* **2008**, 1843. (g) Xu, G.-F.; Wang, Q.-L.; Gamez, P.; Ma, Y.; Clérac, R.; Tang, J.; Yan, S.-P.; Cheng, P.; Liao, D.-Z. *Chem. Commun.* **2010**, 46, 1506. (h) Langley, S. K.; Moubarki, B.; Forsyth, C. M.; Gass, I. A.; Murray, K. S. *Dalton Trans.* **2010**, 39, 1705. (i) Li, D.; Clérac, R.; Parkin, S.; Wang, G.; Yee, G. T.; Holmes, S. M. *Inorg. Chem.* **2006**, *45*, 5251. (j) Murrie, M. *Chem. Soc. Rev.* **2010**, *39*, 1986. (k) Milios, C. J.; Vinslava, A.; Wernsdorfer, W.; Moggach, S.; Parsons, S.; Perlepes, S. P.; Christou, G.; Brechin, E. K. *J. Am. Chem. Soc.* **2007**, *129*, 2754.
- (a) Car, E.-P.; Perfetti, M.; Mannini, M.; Favre, A.; Caneschi, A.; Sessoli, R. *Chem. Commun.* **2011**, 47, 3751. (b) Feltham, H. L. C.; Lan, Y.; Klöwer, F.; Ungur, L.; Chibotaru, L. F.; Powell, A. K.; Brooker, S. *Chem.—Eur. J.* **2011**, *17*, 4362. (c) Chen, G.-J.; Gao, C.-Y.; Tian, J.-L.; Tang, J.; Gu, W.; Liu, X.; Yan, S.-P.; Liao, D. Z.; Cheng, P. *Dalton Trans.* **2011**, 40, 5579. (d) Jiang, S.-D.; Wang, B.-W.; Su, G.; Wang, Z.-M.; Gao, S. *Angew. Chem., Int. Ed.* **2010**, *49*, 7448. (e) Ishikawa, N.; Sugita, M.; Ishikawa, T.; Koshihara, S.; Kaizu, Y. *J. Am. Chem. Soc.* **2003**, *125*, 8694. (f) AlDamen, M. A.; Clemente-Juan, J. M.; Coronado, E.; Marti-Gastaldo, C.; Gaita-Arino, A. *J. Am. Chem. Soc.* **2008**, *130*, 8874. (g) Gonidec, M.; Davies, E. S.; McMaster, J.; Amabilino, D. B.; Veciana, J. *J. Am. Chem. Soc.* **2010**, *132*, 1756. (h) Li, D.-P.; Wang, T.-W.; Li, C.-H.; Liu, D.-S.; Li, Y.-Z.; You, X.-Z. *Chem. Commun.* **2010**, 46, 2929. (i) Jiang, S.-D.; Wang, B.-W.; Sun, H.-L.; Wang, Z.-M.; Gao, S. *J. Am. Chem. Soc.* **2011**, *133*, 4730. (j) Gonidec, M.; Biagi, R.; Corradini, V.; Moro, F.; De Renzi, V.; del Pennino, U.; Summa, D.; Muccioli, L.; Zannoni, C.; Amabilino, D. B.; Veciana, J. *J. Am. Chem. Soc.* **2011**, *133*, 6603. (k) Ishikawa, N.; Sugita, M.; Wernsdorfer, W. *Angew. Chem., Int. Ed.* **2005**, *44*, 2931. (l) Ishikawa, N.; Sugita, M.; Wernsdorfer, W. *J. Am. Chem. Soc.* **2005**, *127*, 3650. (m) Ishikawa, N.; Sugita, M.; Ishikawa, T.; Koshihara, S.; Kaizu, Y. *J. Phys. Chem. B* **2004**, *108*, 11265. (n) Watanabe, A.; Yamashita, A.; Nakano, M.; Yamamura, T.; Kajiura, T. *Chem.—Eur. J.* **2011**, *17*, 7428. (o) Rinehart, J. D.; Meihuis, K. R.; Long, J. R. *J. Am. Chem. Soc.* **2010**, *132*, 7572. (p) Magnani, N.; Apostolidis, C.; Morgenstern, A.; Colineau, E.; Griveau, J.-C.; Bolvin, H.; Walter, O.; Caciuffo, R. *Angew. Chem., Int. Ed.* **2011**, *50*, 1696.
- (a) Mills, D. P.; Moro, F.; McMaster, J.; van Slageren, J.; Lewis, W.; Blake, A. J.; Liddle, S. T. *Nat. Chem.* **2011**, *3*, 454. (b) Rinehart, J. D.; Fang, M.; Evans, W. J.; Long, J. R. *Nat. Chem.* **2011**, *3*, 540. (c) Walter, M. D.; Booth, C. H.; Lukens, W. W.; Andersen, R. A. *Organometallics* **2009**, *28*, 698.
- (a) Evans, W. J.; Johnston, M. A.; Clark, R. D.; Ziller, J. W. *Dalton Trans.* **2000**, 1609. (b) Poremba, P.; Reissmann, U.; Noltemeyer, M.; Schmidt, H.-G.; Brüser, W.; Edelmann, F. T. *J. Organomet. Chem.* **1997**, *554*, 1. (c) Edelmann, A.; Blaurock, S.; Lorenz, V.; Hilfert, L.; Edelmann, F. T. *Angew. Chem., Int. Ed.* **2007**, *46*, 6732. (d) Lorenz, V.; Edelmann, A.; Blaurock, S.; Freise, F.; Edelmann, F. T. *Organometallics* **2007**, *26*, 6681. (e) Summerscales, O. T.; Jones, Cloke, F. G. N.; Hitchcock, P. B. *Organometallics* **2009**, *28*, 5896. (f) Edelmann, F. T. *New J. Chem.* **2011**, *35*, 517 and references therein. (g) Hosoya, N.; Takegami, R.; Suzumura, J.; Yada, K.; Koyasu, K.; Miyajima, K.; Mitsui, M.; Knickelbein, M. B.; Yabushita, S.; Nakajima, A. *J. Phys. Chem. A* **2005**, *109*, 9. (h) Greco, A.; Cesca, S.; Bertolini, G. *J. Organomet. Chem.* **1976**, *113*, 321. (i) DeKock, C. W.; Ely, S. R.; Hopkins, T. E.; Brault, M. A. *Inorg. Chem.* **1978**, *17*, 625. (j) Hodgson, K. O.; Mares, F.; Starks, D. F.; Streitwieser, A. *J. Am. Chem. Soc.* **1973**, *95*, 8650. (k) Schumann, H.; Köhn, R. D.; Reier, F. W.; Dietrich, A.; Pickardt, J. *Organometallics* **1989**, *8*, 1388. (l) Weber, A.; Suhr, H.; Schumann, H.; Köhn, R. D. *Appl. Phys. A: Mater. Sci. Process.* **1990**, *51*, 520. (m) Wayda, A. L.; Cheng, S.; Mukerji, I. *J. Organomet. Chem.* **1987**, *330*, C17. (n) Wayda, A. L.; Mukerji, I.; Dye, J. L.; Rogers, R. D. *Organometallics* **1985**, *4*, 52.
- (a) Bellama, J. M.; Davidson, J. B. *J. Organomet. Chem.* **1975**, *86*, 69. (b) Burton, N. C.; Cloke, F. G. N.; Hitchcock, P. B.; de Lemos, H. C.; Sameh, A. A. *J. Chem. Soc.* **1989**, 1462. (c) Burton, N. C.; Cloke, F. G. N.; Joseph, S. C. P.; Karamallakis, H.; Sameh, A. A. *J. Organomet. Chem.* **1993**, *462*, 39.
- Leng, W. P.; Cheng, H.; Liu, D. S.; Wang, Q. G.; Mak, T. C. W. *Organometallics* **2000**, *19*, 3001.
- (a) Hayes, R.; Edelstein, N. *J. Am. Chem. Soc.* **1972**, *94*, 8688. (b) Boerrigter, P. M.; Baerends, E. J.; Snijders, J. G. *Chem. Phys.* **1988**, *122*, 357. (c) Green, J. C. *Struct. Bonding (Berlin)* **1981**, *43*, 37.
- (a) Becke, A. D. *J. Chem. Phys.* **1993**, *98*, 5648. (b) Lee, C.; Yang, W.; Parr, R. G. *Phys. Rev. B* **1988**, *37*, 785.
- Schafer, A.; Huber, C.; Ahlrichs, R. *J. Chem. Phys.* **1994**, *100*, 5829.
- (a) Dolg, M.; Stoll, H.; Preuss, H. *Theor. Chem. Acc.* **1993**, *85*, 441. (b) Cao, X. Y.; Dolg, M. *J. Chem. Phys.* **2001**, *115*, 7348. (c) Cao, X. Y.; Dolg, M. *Theo. Chem.* **2002**, *581*, 139.
- (a) Mayer, I. *Int. J. Quantum Chem.* **1986**, *29*, 73. (b) Gorelsky, S. I.; Basumallick, L.; Vura-Weis, J.; Sarangi, R.; Hedman, B.; Hodgson, K. O.; Fujisawa, K.; Solomon, E. I. *Inorg. Chem.* **2005**, *44*, 4947.
- Gatteschi, D.; Sessoli, R.; Villain, J. *Molecular Nanomagnets*; Oxford University Press: New York, 2006 and references therein.